Tellus (2000), 52B, 439–451
Printed in UK. All rights reserved

TELLUS
ISSN 0280–6509

A simple non-linear analytical relationship between aerosol accumulation number and sub-micron volume, explaining their observed ratio in the clean and polluted marine boundary layer

By RITA VAN DINGENEN[1]*, AKI O. VIRKKULA[1], FRANK RAES[1], TIMOTHY S. BATES[2] and ALFRED WIEDENSOHLER[3], [1]*European Commission, Joint Research Centre, Environment Institute, T.P. 460, I-21020 Ispra (VA), Italy;* [2]*NOAA/Pacific Marine Environmental Laboratory (PMEL), 7600 Sand Point Way, NE, Seattle, Washington 98115, USA;* [3]*Institute for Tropospheric Research, Permoserstrasse 15, D-04303 Leipzig, Germany*

(Manuscript received 19 May 1999; in final form 13 September 1999)

ABSTRACT

We propose an analytical expression for the relation between aerosol accumulation number and sub-micron volume over the marine boundary layer (MBL), based on a simple balance equation. By providing appropriate source and sink terms which account for entrainment, coagulation, in-cloud scavenging and condensational growth, the model is able to reproduce the observed ratio between MBL particles larger than 80 nm diameter (as a proxy for accumulation mode number) and submicron aerosol volume, from freshly polluted to background conditions. Entrainment and coagulation are essential in predicting the observed ratio. Budget and lifetime calculations show that, due to relatively low source rates of oceanic non-sea-salt-sulfate and sea-salt, the anthropogenic signature in aerosol volume remains significant even after 8 days of MBL transport.

1. Introduction

One of the major goals of the ACE-2 experiment was to study the processes and rates that govern the transformation of anthropogenic aerosols into the remote marine aerosol (Raes et al., 2000). A better understanding of these processes should then guide their implementation into global models, evaluating the direct and indirect effect of anthropogenic aerosols on the atmosphere's radiation budget.

A number of studies of marine aerosol properties have shown that, away from the continental source areas, number size distributions evolve into an Aitken and accumulation mode with stable mean geometric diameters and an inter-modal minimum round 60–80 nm (Hoppel et al., 1985, 1986, 1994; Van Dingenen et al., 1995, Porter and Clarke, 1997; Raes et al., 1997). This stable shape is a consequence of aqueous phase chemistry in non-precipitating clouds acting on a relatively chemically uniform marine boundary layer (MBL) aerosol, coupled with a limited range of supersaturations prevailing in the commonly occurring stratiform clouds over the oceans (Hoppel et al., 1986; Fitzgerald et al., 1998). Furthermore, Raes (1995) suggested, based on a modelling study, that the constant number concentrations in the remote

* Corresponding author.
e-mail: rita.van-dingenen@jrc.it
† Present affiliation: Finnish Meteorological Institute, Air Quality Research, Sahaajankatu 20E, FIN-00810 Helsinki, Finland.

MBL are driven by entrainment from the overlaying free troposphere (FT). Observations and modelling of clean and perturbed air masses over the North Atlantic have given additional support to this hypothesis, by explaining the observed aerosol number and volumes in terms of their residence times over the ocean and by dilution with entrained FT air (Van Dingenen et al., 1999).

An interesting aspect of this relatively stable MBL aerosol is the quasi constant ratio between the number of particles with diameter larger than 80 nm (N_{80}) which can be considered as potential cloud condensation nuclei (CCN) at supersaturations prevailing in the MBL (Pruppacher and Klett, 1978; Hoppel et al., 1996) and (submicron) aerosol volume (V_{sm}). A simple relationship between N_{80} and V_{sm} is a great advantage in the calculation of the cloud droplet number in stratiform clouds resulting from increased (anthropogenic) emissions in global models, as it could bypass expensive aerosol dynamics modelling to relate emissions to aerosol number. Previous field studies in the perturbed and clean MBL (Hegg and Kaufman, 1998 (HK98); Van Dingenen et al., 1999 (VD99)) have shown that N_{80}/V_{sm} is close to 200 μm^{-3} with V_{sm} ranging between 0.1 and 10 $\mu m^3\,cm^{-3}$, implying a near-linear relation between N_{80} and V_{sm} HK98 suggested that this constant ratio was a consequence of sulfate and organic condensational growth on different particle sizes, such that sulfate provides rather a source for N_{80} (by nucleation and condensational growth) and organic material for mass or volume (preferably condensing on pre-existing larger particles), preserving their ratio. VD99 explained the constancy by the dominance of entrainment of clean FT air over other MBL aerosol processes when pollution advects over the ocean. As FT air has very low N_{80} and V_{sm}, entrainment basically acts as a simultaneous dilution process for N_{80} and V_{sm}, reducing their absolute values but not their ratio.

An important question which was not really solved in these studies is how the value $N_{80}/V_{sm} = 200\ \mu m^{-3}$ is established in the MBL, as it is not a universal value over the continental source areas. In this paper we further investigate this relation, making use of aerosol distribution measurements in the remote as well as polluted MBL from different platforms during ACE-2, eventually providing a useful parameterisation that reflects the contribution of various aerosol processes onto the N_{80}–V_{sm} relationship.

2. Experimental

The dataset considered consists of sub-micron size distributions measured at 4 stations during ACE-2:

(a) Punta Del Hidalgo (PDH, located in the MBL) and Izaña observatory (IZO, located in the FT), Tenerife (Van Dingenen, R.; Raes, F.; Virkkula, A. Aerosol size distributions in the marine boundary layer and free troposphere at Tenerife, Canary Islands, manuscript in preparation, hereafter referred to as: Van Dingenen et al., manuscript in preparation)

(b) Research ship RV Professor Vodyanitskiy (VOD) (Bates et al., 2000).

(c) Sagres, Portugal (SAG) (Neusüß et al., 2000)

For a detailed description of instrumentation and techniques, the reader is referred to the respective references given. The geographical location of the platforms is shown by Verver et al. (2000). Of the three locations, Tenerife is the most remote site. During ACE-2, three MBL pollution outbreaks from Europe were observed in PDH, which, according to air mass trajectories, needed 40–60 h transport time over the ocean before reaching the island. Also episodes with more aged but still perturbed air masses were sampled (see also Putaud et al. (2000)). Measurements from IZO in the FT (2360 m asl) are also included in the present dataset to document the properties of aerosols that are entrained in the MBL. Sagres, on the Portuguese SE coast, is frequently impacted by fresh pollution aerosol. In fact, the site observed local and transported polluted air masses almost continuously in the second half of the experiment. Verver et al. (2000) discuss the difference between PDH and SAG in aerosol loading and frequency of pollution impacts. The *RV Professor Vodyanitskiy* operated in the area between 30° and 40°N and east of 15°W, i.e. roughly between Tenerife and Sagres. It was sampling in clean as well as fresh and aged polluted air masses, of which the freshest ones have spent less than 1 day over the ocean.

Aerosol size distributions were measured on all 3 platforms with DMA techniques, which are described by the respective references given above.

The dataset discussed in this paper consists of integrated number concentrations of particles with diameter between 80 and 500 nm (N_{80}), and integrated aerosol volume (V_{sm}) below 500 nm. The size distributions have been measured at or reduced to dry conditions (10% RH).

It should be noted that our instrumentation differs from the one used by HK98: their size distributions were obtained with a passive cavity aerosol spectrometer, measuring sizes between 0.12 and 3 μm. Hence, for identical size distributions, HK98 would in general report higher volumes and lower N, resulting in lower N/V values than in our study. The amount of V_{sm} "missed" by the DMA cut-off at 500 nm is estimated by fitting bimodal lognormal functions to a number of averaged and representative distributions, covering the whole range of aerosol volumes encountered. The integral fitted volume can then be compared with the measured volume below the DMA cut-off. Fig. 1 shows examples of (a) measured and fitted number size distributions, (b) corresponding measured and fitted volume distributions, the latter extrapolated beyond the DMA cut-off and (c) the relation between DMA derived volume and extrapolated volume. This analysis shows that, from clean to polluted cases, 3 to 15% of V_{sm} is not measured by the DMA. On the other hand, because of the lower cut-off at 120 nm, HK98 would miss 10% (clean) to 2% (polluted) of V_{sm} in the same situation. The effect of the upper DMA cut-off on number is negligible, whereas the 120 nm lower cut-off of HK98 would detect 40% (clean) to 10% (polluted) less accumulation mode particles compared to N_{80}. The combined effect leads to N_{80}/V_{sm} in our study which is around 30% higher than what would be measured with HK98s system, provided that an additional coarse mode is not contributing significantly to the latter. In the following, reported experimental V_{sm} values refer to the 6–500 nm size range. Furthermore, it has to be noted that we report

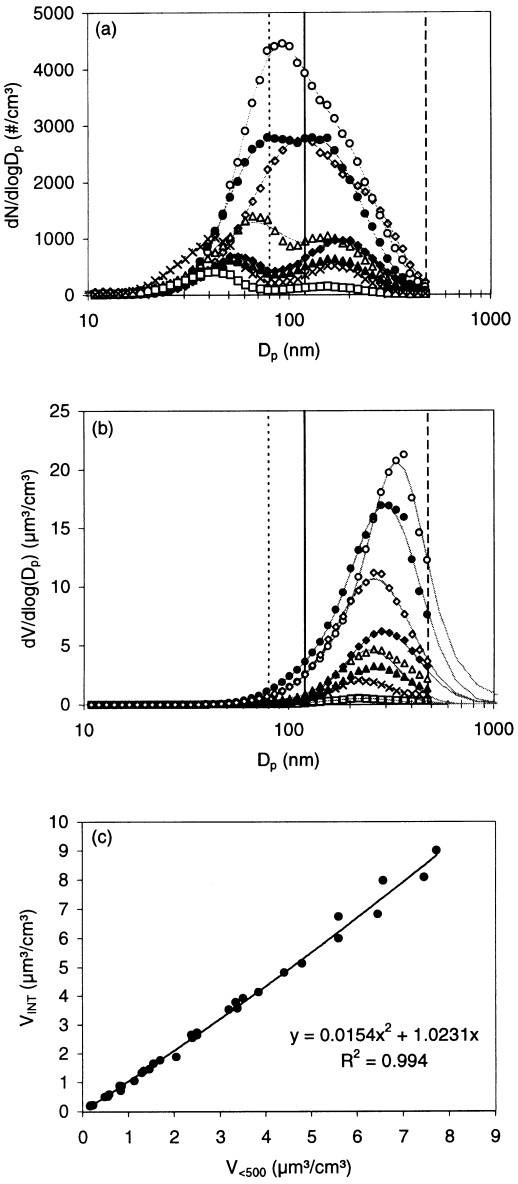

Fig. 1. (a) Examples of typical number size distributions measured at PDH (Tenerife) during ACE-2 (symbols), together with a fitted bimodal lognormal function (lines). Different curves show the transition from clean, background air to polluted plumes advected from Europe. The vertical lines cut the distribution at 80 nm (dotted line) and 500 nm (dashed line), i.e., the lower and upper cut-off for N_{80} and V_{sm} (this work), and at 120 nm (full line), i.e. the lower cut-off for N_{120} (Hegg and Kaufmann, 1998). (b) Volume size distributions for the same distributions as in (a), together with the lognormal fittings converted to dV/d log D_p. The lognormal curves have been extended beyond the measured upper diameter, in order to estimate the missing volume fraction. (c) Relation between aerosol volume within the measurement range ($V < 500$) and total integrated volume (V_{INT}).

N_{80}/V_{sm} as individual values for each measured distribution, whereas HK98 obtain this ratio as the slope of a linear regression line through a number of points. In HK98 as well as this study, aerosol volume is that of dry aerosol.

The present dataset is an extension of the remote MBL data discussed in VD99, as it also includes fresh pollution aerosol over the MBL. This dataset allows us to update the assumed initial conditions of the pollution aerosol, and to investigate the constancy or variability in the N_{80}/V_{sm} ratio for fresh pollution. Rather than plotting N_{80} versus V_{sm}, we will explore the variation with V_{sm} of the ratio N_{80}/V_{sm}, which enhances the signal in the data.

Having calculated for each individual size distribution of all platforms the ratio N_{80}/V_{sm}, we constructed in Fig. 2 contour plots of the frequency of occurrence of N_{80}/V_{sm} versus V_{sm} for each of the 3 sites (the Tenerife plot contains data from PDH and IZO). Also shown are lines of constant N_{80}. The plots show some interesting features that can be understood in terms of aerosol processes. Tenerife data (Fig. 2a) are the most homogeneous and most confined dataset. As already noticed in the previous studies by HK98 and VD99, the N_{80}/V_{sm} ratio is approximately 200 μm^{-3}. However, Fig. 2a shows that in the MBL, N_{80}/V_{sm} decreases with increasing V_{sm}, which is a refinement of our previous statement that N_{80}/V_{sm} is quasi constant. N_{80}/V_{sm} in the FT is significantly higher, and FT data result as a clearly detached cluster with N_{80}/V_{sm} around 500 μm^{-3}, "connected" more or less along a N_{80} isoline to the MBL data. This is consistent with entrainment of small FT aerosol (broad unimodal distribution at approximately 60 nm, low volume) into the MBL with a sharp activation at 80 nm, after which the aerosol grows by cloud processing (i.e., same N_{80} in FT and MBL). Condensation onto Aitken mode particles is a source for accumulation mode number and volume and hence will move the endpoint towards higher N_{80}. Rainout and washout on the other hand will reduce N_{80} and V_{sm} along a constant N_{80}/V_{sm} line, whereas production of accumulation mode sea-spray particles would work in the opposite direction. The three pollution outbreaks detected at Tenerife are visible as the three clusters on the $N_{80} = 1600$ isoline. The highest N_{80}/V_{sm} ratio of the 3 cases corresponds to air masses that came off the Iberian Peninsula 36 h before, whereas the other two pertain to more aged polluted air masses from N. Europe. These points illustrate what appears more clearly in the VOD and SAG plots, namely that N_{80}/V_{sm} increases again in air masses which are less aged.

Ship and Sagres data are more scattered than PDH data, but nevertheless they show the highest frequency for N_{80}/V_{sm} around 200 μm^{-3}, even at

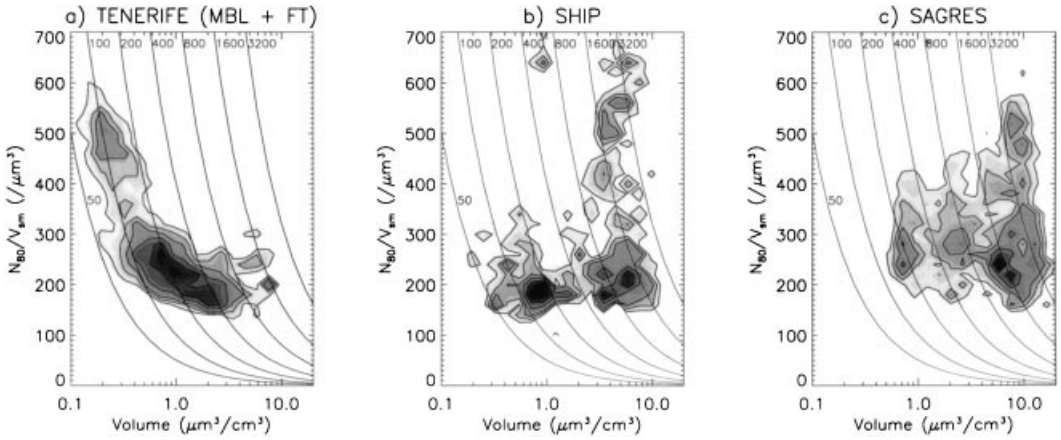

Fig. 2. Contour plots of the frequency of occurrence of N_{80}/V_{sm} for 3 ACE-2 platforms: (a) Tenerife (PDH and IZO), (b) R/V Vodyanitskiy, (c) Sagres, Portugal. N_{80} is the number of particles larger than 80 nm diameter, V_{sm} is the integrated sub-micron aerosol volume. Dark shades indicate higher frequencies. Full lines are isolines of N_{80} concentration (number indicates the concentration (cm^{-3}).

high V_{sm}. The figure also shows that much higher values, up to 700 μm^{-3}, can prevail, with increasing frequency when getting closer to the pollution source (as indicated by high aerosol volume). Backtrajectory analysis for the ship shows that the "string" of high N_{80}/V_{sm} values at high V_{sm} all pertain to air masses coming off the Iberian Peninsula, having spent a few h over the ocean, depending on the position of the ship. The cluster of low N_{80}/V_{sm} values at high V_{sm} pertain to polluted air masses from N. Europe, which advected over the ocean for more than 30 h, comparable to the pollution cases in Tenerife. Interestingly, a simple analysis of N_{80}/V_{sm} using an analytical lognormal number distribution, limiting the geometric standard deviation σ_g to the range 1.4 to 2, shows that $N_{80}/V_{sm} = 700\ \mu m^{-3}$ is only possible for a geometric mean diameter D_{pg} lower than 110 nm, whereas $N_{80}/V_{sm} = 200\ \mu m^{-3}$ is possible for D_{pg} between 80 and 180 nm. As accumulation mode dry diameters in the MBL are usually above 120 nm (Bates et al., 2000), a high N_{80}/V_{sm} value, in combination with high V_{sm}, indicates freshly produced (secondary) aerosol in a pollution plume, consistent with our observations.

The VD99 study already indicated that the linear relationship between N_{80} and V_{sm} (i.e., the constant N_{80}/V_{sm} ratio) does not hold in fresh pollution. The study also indicated that the modelled N_{80}/V_{sm} over the ocean is quite sensitive to the initial N_{80}/V_{sm} of the pollution aerosol, and good agreement between observed and modelled N_{80} and V_{sm} was obtained only for an initial pollution aerosol $N_{80}/V_{sm} = 250$, which is however not the general situation as appears from Fig. 2.

In the following, we envisage a more general parameterisation of the N_{80} versus V_{sm} relationship in terms of physical process parameters like source and sink rates, which would capture the observed trends in remote as well as polluted areas.

3. Parameterisation of N_{80} versus V_{sm} in the MBL

We describe the ageing of initial pollution aerosol over the ocean, starting from the following balance equations for N_{80} and V_{sm}:

$$\frac{dN_{80}}{dt} = S_N - \lambda_N N_{80} - K N_{80}^2, \tag{1}$$

$$\frac{dV_{sm}}{dt} = S_V - \lambda_V V_{sm}. \tag{2}$$

S_N and S_V represent the source terms for N_{80} and V_{sm}, respectively. This includes sea spray, condensation and cloud chemistry, and entrainment from the FT. λ_N and λ_V are loss terms including dilution and wet deposition (depositing drizzle), in-cloud scavenging and coalescence. K is a rate constant for coagulation outside clouds. If all rate constants represent averages over the aerosol lifetime, the solution for N_{80} and V_{sm} is given by:

$$N_{80} = \frac{1}{2K}\left[A\left(\frac{B + e^{-At}}{B - e^{-At}}\right) - \lambda_N \right], \tag{3}$$

$$V_{sm} = V_0\, e^{-\lambda_V t} + V_\infty (1 - e^{-\lambda_V t}), \tag{4}$$

where

t = time since the air parcel left the continent,

$$V_\infty = \frac{S_V}{\lambda_V},$$

$$A = \sqrt{\lambda_N^2 + 4KS_N},$$

$$B = \frac{2KN_0 + \lambda_N + A}{2KN_0 + \lambda_N - A}.$$

N_0, V_0 = initial N_{80} and V_{sm} of the pollution aerosol when leaving the continent. Eliminating t from eqs. (3) and (4) gives N_{80} as a function of V_{sm}:

$$N_{80} = \frac{1}{2K}\left[\frac{B(A - \lambda_V)(V_{sm} - V_\infty)^{-A/\lambda_V} + (A + \lambda_N)(V_0 - V_\infty)^{-A/\lambda_V}}{B(V_{sm} - V_\infty)^{-A/\lambda_V} - (V_0 - V_\infty)^{-A/\lambda_V}} \right]. \tag{5}$$

Table 1 gives an overview of the parameter values used in the model. The choice for the adopted values is discussed in Section 7. Fig. 3 shows the analytically calculated N_{80}/V_{sm} ratio versus V_{sm} of an evolving pollution plume, together with Tenerife and ship N_{80}/V_{sm}. Two types of initial conditions have been used as limiting cases, based on the Sagres observations: initial N_{80}/V_{sm} near 650 μm^{-3}, and initial N_{80}/V_{sm} near 350 μm^{-3}, respectively. Apart from the initial conditions, the two curves differ by the applied coagulation rate,

Table 1. *Overview of parameters and rate constants used in the analytical model for the two limiting cases (case 1–case 2) and variation is some parameters for sensitivity analysis (S1–S7), together with resulting N_{80}/V_{sm} ratio, residence times and equilibrium concentrations for N_{80} and V_{sm}*

Parameter and unit	Symbol	Case 1	Case 2	S1	S2	S3	S4	S5	S6	S7
entrainment velocity ($cm\ s^{-1}$)	ω	0.65		0.3						
MBL height (m)	H	1000								
coalescence + scavenging (s^{-1})	λ_c	1×10^{-6}							0	
wet + dry deposition (s^{-1})	λ_d	5×10^{-7}						0		
coagulation ($cm^3\ s^{-1}$)	K	2×10^{-9}	7×10^{-10}							
condensation + cloud processing source rate V_{sm} ($\mu m^3\ cm^{-3}\ s^{-1}$)	$S_{V,CON}$	10^{-6}				2.5×10^{-6}				
condensation source rate N_{80} ($cm^{-3}\ s^{-1}$)	$S_{N,CON}$	10^{-4}					3×10^{-4}			
sea salt total N production rate ($cm^{-3}\ s^{-1}$)		3×10^{-4}								3×10^3
sea-salt D_{pg} (nm)		120								
sea-salt σ_g		1.5								
sea salt source rate N_{80} ($cm^{-3}\ s^{-1}$)		2.5×10^{-4}								
sea-salt source rate V_{sm} ($\mu m^3\ cm^{-3}\ s^{-1}$)		5.7×10^{-7}								
MBL pollution aerosol N_{80} (cm^{-3})	N_0	4000	7000							
MBL pollution aerosol V_{sm} ($\mu m^3\ cm^{-3}$)	V_0	6	20							
FT N_{80} (cm^{-3})	N_{FT}	100			50					
FT V_{sm} ($\mu m^3\ cm^{-3}$)	V_{FT}	0.2			0.1					
N_{80}/V_{sm} ($t = 60$ h) (μm^{-3})		288	193	169	190	187	197	190	231	210
N_{80} e-folding residence time (h)	τ_N	33.7	34.4	60.4	34.5	34.4	34.3	36.6	39.1	33.6
V_{sm} e-folding residence time (h)	τ_V	39.7	39.7	79.4	39.7	39.7	39.7	42.7	39.7	39.7
equilibrium concentration N_{80} (cm^{-3})	N_∞	122	124	142	84	124	148	132	141	396
equilibrium concentration V_{sm} ($\mu m^3\ cm^{-3}$)	V_∞	0.41	0.41	0.62	0.32	0.62	0.41	0.44	0.41	1.14

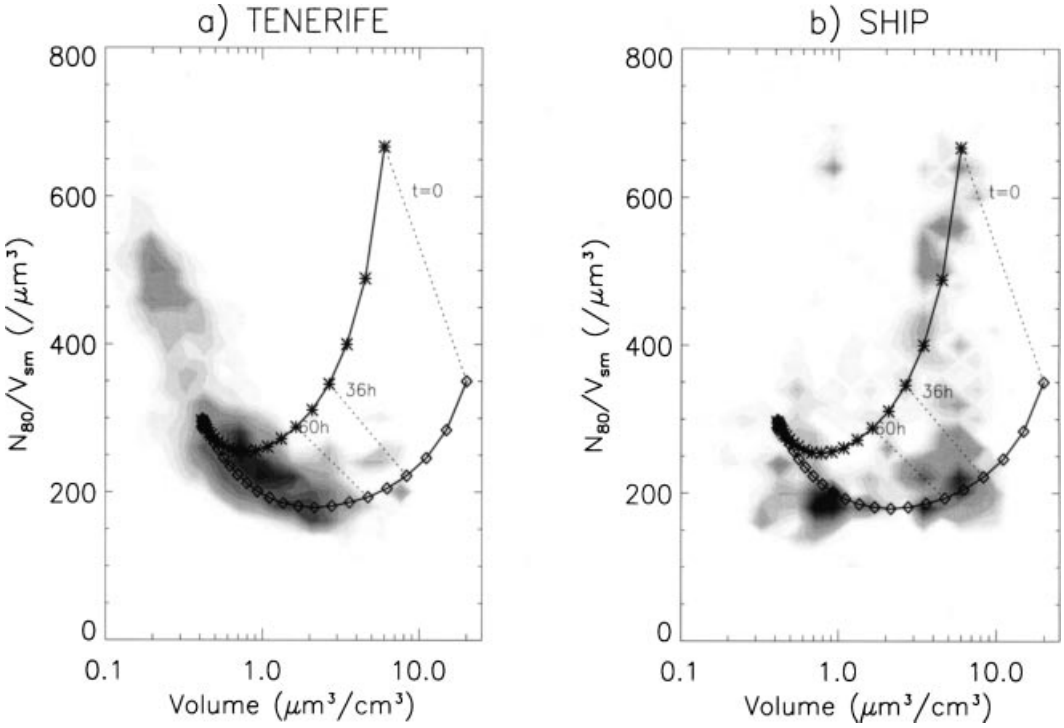

Fig. 3. Result of the analytical model, showing N_{80}/V_{sm} against V_{sm} (full line), for 2 limiting cases of a pollution aerosol leaving the continent and ageing in the MBL (see text and Table 1). Model results are plotted over the experimental data for N_{80}/V_{sm} for Tenerife (a) and ship (b) (same data as in Fig. 2). Symbols on the line are 12-h intervals for the aerosol evolving from high (indicated by $t = 0$) to low V_{sm}. Dotted lines connect the modelled N_{80}/V_{sm} for the 2 cases after 36 and 60 h of ageing.

the upper curve being more representative for freshly produced aerosol with smaller particle size, hence faster coagulation (see Section 7). The symbols on the curves represent 12-h interval data points, with the initial situation at the right hand side of the curves, indicated by $t = 0$. We want to stress that in this analysis, we do not consider ship and Tenerife to be connected by the same air flow, nor that the experimental data in each of the sites are obtained in one evolving plume. We assume that during the measurement period, both sites are sampling aerosol of varying age, and of varying origin, with the highest aerosol volumes occurring in air masses advecting of the Iberian peninsula. The model is used to explain in a consistent way the relation between N_{80} and V_{sm} in this range of air mass conditions for the 2 sites.

It appears that the simple model can capture the general trend in the data, in particular the minimum of the N_{80}/V_{sm} ratio when V_{sm} is between 1 and 4 $\mu m^3/cm^3$. This broad minimum, where N_{80}/V_{sm} is close to 200 μm^{-3}, coincides with the V_{sm} range covering 90% of the observations on Tenerife, which explains the quasi-linear trend in the experimental data. The model also explains the range of high N_{80}/V_{sm} ratios observed at the ship when it was close to the continent (between 0 and 24 h residence time of the air mass over the ocean), and the lack of occurrence of these high values in Tenerife due to its distance downwind of the source area. The majority of Tenerife data are reproduced by the model after 60 h or more ageing time, in agreement with air mass back-trajectories.

The N_{80}/V_{sm} ratio at the minimum is governed by the relative magnitude of entrainment and coagulation rates. When the particle concentration has decayed far enough for coagulation to fade out, entrainment will preserve the prevailing N_{80}/V_{sm} by further diluting both N_{80} and V_{sm}, until

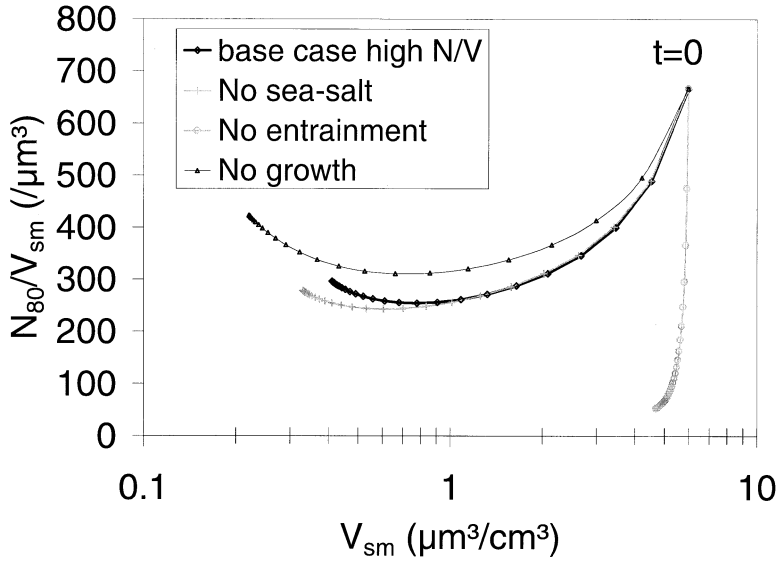

Fig. 4. Effect of various processes on the N_{80}/V_{sm} ratio as function of V_{sm} from the analytical model (case 2 only). Symbols indicate 12-h intervals when the aerosol evolves from high to low V_{sm} over 14 days transport in the MBL. Results are similar for case 1.

the ratio of entrained FT aerosol becomes significant. A lower entrainment rate allows coagulation to go on for a longer time and will result in a lower N_{80}/V_{sm}.

Fig. 4 illustrates the importance of simultaneous coagulation and entrainment in establishing the observed N_{80}/V_{sm} ratio attained during a 14 days-transport of pollution aerosol in the MBL; without dilution by entrainment of FT aerosol, V_{sm} does not reduce to the low values observed in the remote MBL. The only processes to reduce V_{sm} in that case are drizzle and dry deposition.

Sea-salt production is affecting the N_{80}/V_{sm} ratio only in clean conditions. The production rate affects the steepness of the curve and the maximum N_{80}/V_{sm} reached at low V_{sm}. Part of the variability in N_{80}/V_{sm} in clean conditions may be ascribed to the variability in sea-salt production, but the effect appears to be rather small.

Without condensation, lower aerosol volumes and hence a higher N_{80}/V_{sm} result, but the process is not critical in establishing the observed relationship.

The sensitivity of the modelled N_{80}/V_{sm} to the input parameters is further explored in Table 1. The first two columns correspond to the 2 curves shown in Fig. 3. The values in the other columns are changes with respect to column 1. This analysis shows that after 60 h of ageing, N_{80}/V_{sm} is most sensitive to the coagulation rate and entrainment velocity, as discussed before. The variations in condensation rate, deposition and scavenging rates, as well as in sea-salt production, do not lead to large excursions of N_{80}/V_{sm} from the base case, explaining the homogeneity of the experimental data in Tenerife.

4. Budget calculations and residence times in the MBL

By applying the analytical models (3) and (4) to each of the MBL aerosol sources (transported pollution, sea-salt, FT and condensation + cloud processing), we can evaluate the contribution of each of them to N_{80} and V_{sm}. Fig. 5 shows the respective fractions in the aerosol volume (a, b) and number (c, d) as a function of transport time for the two modelled limiting cases. It is surprising to see that the initial pollution aerosol, transported in the MBL, still makes up more than 50% of the aerosol volume after 5–6 days of transport time, i.e., when the absolute aerosol volume concentration is reduced to less than 10% of its initial value.

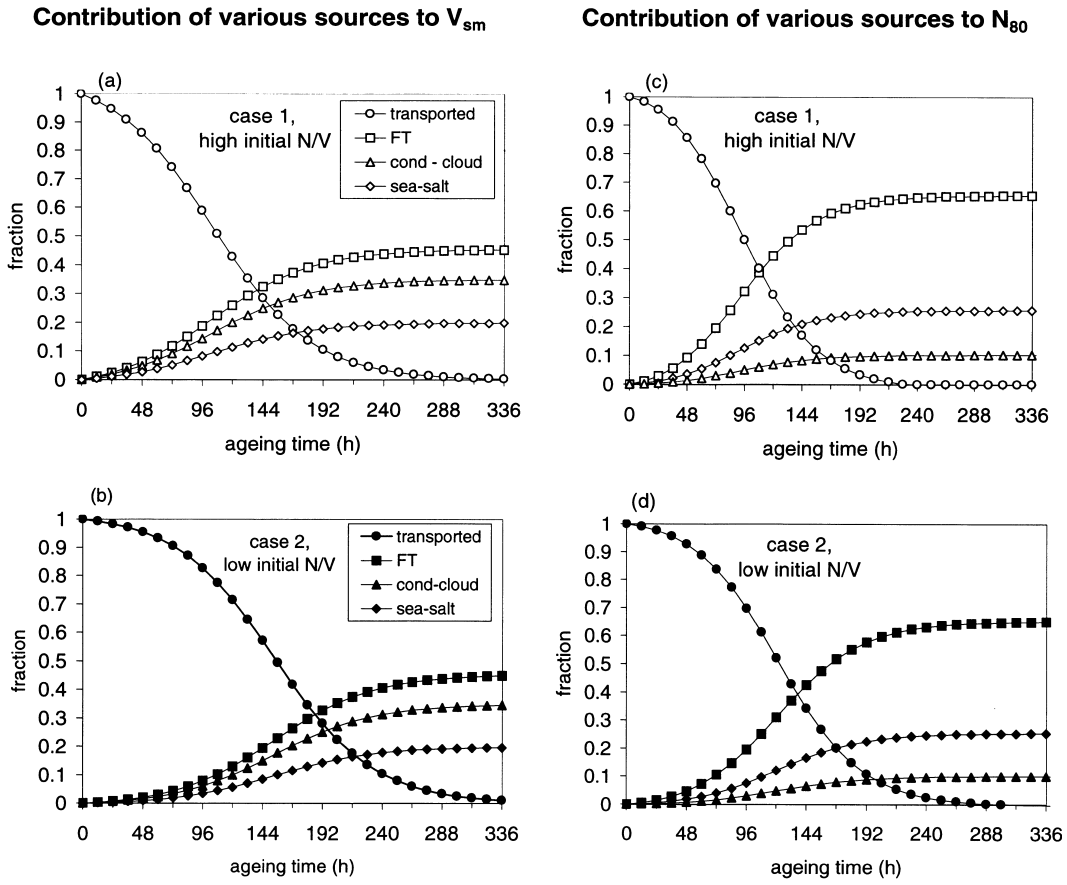

Fig. 5. Relative contribution of various sources to the aerosol volume (a) and (b) and number larger than 80 nm (c) and (d) as a function of ageing time, for the 2 limiting cases calculated with the analytical model. Symbols on the lines are at 12-h intervals when the aerosol evolves from polluted to clean conditions.

This is a consequence of the low aerosol number and volume entrained from the FT and slow in-situ growth such that the anthropogenic aerosol is diluted, without rapidly being replaced. In the cleanest conditions, about 45% of the aerosol volume has originated in the FT, 35% consists of condensed material in the MBL and 20% of sea-salt. As the entrained aerosol is also subject to losses in the MBL, the maximum FT contribution in the MBL corresponds to 85% of the FT aerosol volume.

The anthropogenic fraction in N_{80} decreases more rapidly than for V_{sm}, but still a 50% contribution can be seen after 4 to 5 days transport time (Fig. 5c, d). The anthropogenic contribution in N_{80} becomes $<10\%$ after 6 to 7 days, for V_{sm} after 8 to 9 days. Equilibrium concentrations for N_{80} and V_{sm} are given by

$$N_\infty = \frac{A - \lambda_N}{2K} \qquad \text{and} \qquad V_\infty = \frac{S_V}{\lambda_V},$$

yielding background values for N_{80} and V_{sm} of 115 cm^{-3} and 0.38 $\mu m^3/cm^3$ respectively. Dividing these equilibrium concentrations by the respective production rates, gives *e*-folding turn-over times of 34 h for N_{80} and 40 h for V_{sm}. These values can be compared with the ones obtained by Ackerman et al. (1994) who applied a detailed aerosol and cloud process model to evaluate CCN concentrations in a cloud topped MBL. These authors obtain a residence time for aerosol mass (or volume) which is comparable to ours (for a

$100\ cm^{-3}$ CCN equilibrium concentration), but find only 12 h for CCN number. This is due to the fact that they assume a 100% cloud cover, and consequently overestimate cloud scavenging of aerosol number. Furthermore, they do not consider entrainment as an additional dilution process for MBL aerosol. In such conditions, the large difference in number and volume residence times could not lead to a constant N_{80}/V_{sm} ratio over a large range of aerosol volumes.

Table 1 also gives the turn-over times and equilibrium concentrations for N_{80} and V_{sm} for the 2 modelled cases and varying some of the process rates. The present simple model confirms the conclusion from VD99, namely that entrainment is the major process governing the residence time of aerosol number and volume in the MBL.

Fig. 5c, d also show that entrainment of FT aerosol remains the major source of N_{80}, followed by sea-salt. Although the FT is usually seen as a source for Aitken model particles in the MBL, the broad FT aerosol number size distribution extends far enough beyond 80 nm to provide a significant source of accumulation mode particles (Raes et al., 1997), in general stronger than sea-salt in the submicron size range. Sea-salt has been detected in submicron aerosol down to 50 nm (O'Dowd and Smith, 1993; Murphy et al., 1998) but an adequate description of the number size distribution in the submicron size range is still lacking. The rather narrow size distribution round 120 nm in our simulation can be considered as an upper limit for the number of sea-salt particles larger than 80 nm per unit of sea-salt mass. The rightmost column of Table 1 has been calculated for a tenfold sea-salt production rate. Although not being typical for the experimental conditions in this study, such values have been observed during ACE-2. In such conditions, sea-spray can become the major source for particle number in the MBL (Hoell et al., 2000).

5. Conclusions

With a simple analytical model, we have been able to reproduce observed concentrations of potential CCN (here defined as particles larger than 80 nm) and aerosol volume in the MBL, as well as their ratio for aged and freshly polluted air masses. High N_{80}/V_{sm} ratio's, observed in fresh pollution aerosol, are never observed 36 h–60 h downwind the pollution source. This is explained by rapid decay through coagulation in those plumes, which are characterised by a high aerosol number concentration. In-cloud scavenging of interstitial aerosol and cloud drop coalescence are probably significantly contributing to this number decay. Entrainment remains an essential process in further reducing number and volume, and in preserving the established N_{80}/V_{sm} ratio, once coagulation had died out. Both processes tend to "linearise" the effect of increased emissions on the number of potential CCN; in other words, the strong variability in continental aerosol is rapidly quenched when the aerosol travels over the ocean.

The obtained analytical expression is a useful step in the parameterisation of the number of cloud droplets in terms of increased anthropogenic emissions. In order to be applicable in large-scale models that generally compute fields of aerosol mass, an additional relation between aerosol volume and mass (or a major mass component, like sulfate) is needed. The chemical closure experiments which have successfully been conducted during ACE-2 (Putaud et al., 2000; Neusüß et al., 2000) provide this required information.

6. Acknowledgements

This research is a contribution to the International Global Atmospheric Chemistry (IGAC) Core Project of the International Geosphere–Biosphere Programme (IGBP) and is part of the IGAC Aerosol Characterization Experiments (ACE). It has been supported by EC contract no ENV4-CT95-0140 (FREETROPE).

7. Appendix

Process rate constants used in the analytical N_{80}–V_{sm} model

7.1. Entrainment

Entrainment from the FT is described through a single entrainment velocity ω between FT and MBL. MBL air is flushed with FT aerosol, with concentration N_{FT} and aerosol volume V_{FT}. It acts as a dilution process for N_{80} and V_{sm} with rate $-\omega/H$ and simultaneously injects FT aerosol in

the MBL at a source rate $N_{FT}\omega/H$ and $V_{FT}\omega/H$, respectively. For the base case, we used an entrainment velocity of 0.65 cm/s (Bretherton et al., 1995). Number and volume of FT aerosol are 100 cm^{-3} and 0.2 respectively, in agreement with the observations shown in Fig. 2.

7.2. Sea salt

Sea-salt production is described by assuming a lognormally distributed number ($D_{pg} = 120$ nm, $\sigma_g = 1.5$), produced at a rate 3×10^{-4} particles/cm^3/s for the base case. The source rate for the volume is obtained by multiplying the production rate with the integrated volume of the distribution; the source rate for N_{80} is obtained by taking only the cumulative concentration >80 nm of the distribution times the total production rate. Hence, depending on the geometric mean diameter and standard deviation, different rates for number and volume can result. For the given distribution parameters, the adopted particle production rate was constrained as to yield the observed 20% volume fraction of sea-salt in the submicron aerosol in clean conditions (Putaud et al., 2000).

7.3. Coagulation

Assuming accumulation mode aerosol at ambient humidity round 230 nm (dry diameter = 170 nm (Bates et al., 2000); growth factor to ambient humidity = 1.38 (Swietlicki et al., 2000)) and standard deviation = 1.45 (Bates et al., 2000), a polydisperse rate of 7×10^{-10} $cm^3\,s^{-1}$ is adopted. This rate is taken as the lower limit for coagulation processes in the model. As an upper limit we adopt $K = 2 \times 10^{-9}$ $cm^3\,s^{-1}$, assuming fresh pollution aerosol with ambient humidity diameter = 110 nm and σ_g between 1.5 and 2, as observed in Sagres. Both rates result from Hinds, 1982.

7.4. Cloud coagulation and coalescence

Coalescence and below cloud scavenging with re-evaporation before the surface is reached, can be very efficient in removing particle number without affecting volume, but these processes are more difficult to estimate. Scavenging and coalescence rates are usually expressed as a loss rate with $[t]^{-1}$ dimension (Pruppacher and Klett, 1978; Seinfeld and Pandis, 1998). For a cloud frequency of 1 cloud every 9 h, and a 20% volume occupancy of the MBL, coagulation between interstitial aerosol and cloud droplets leads to a loss rate of the order $5 \times 10^{-7}\,s^{-1}$. We have rather arbitrarily doubled this value to include coalescence and below-cloud scavenging of non-precipitating drizzle. This loss rate does not affect the aerosol volume.

7.5. Dry and wet deposition

The dry deposition rate for accumulation mode aerosol particles, taken from Slinn et al. (1978), is not exceeding $10^{-7}\,s^{-1}$. The wet deposition rate is estimated as follows: according to Seinfeld and Pandis (1998), the scavenging coefficient per mm rainfall for accumulation mode particles by 0.4 mm raindrops is around $10^{-3}\,mm^{-1}$. The rainfall rate in the ACE-2 area for July 1997 is below 50 mm per month (Global Precipitation Climatology Project GPCP, 1999; Huffman et al., 1997), resulting in a wet deposition rate for number and volume of $2 \times 10^{-7}\,s^{-1}$. In the model we have adopted a value of $5 \times 10^{-7}\,s^{-1}$ as upper limit for combined wet and dry loss rate.

7.6. Condensation and aqueous phase chemistry

Aqueous phase chemistry during cloud events is the major process adding mass to existing CCN. Furthermore, condensation is an additional source for both V_{sm} and N_{80}, in the latter case by growing Aitken mode over the 80 nm boundary. The source rate for aerosol volume by condensation and cloud processing is estimated by assuming that the volume growth is limited by production of H_2SO_4 from SO_2 in the aqueous phase and from photochemistry, respectively. Hence, condensation and cloud processing source rates for the volume are given by:

$$S_{V,CON} \times \frac{f_c k_1}{\rho}[OH][SO_2], \tag{6}$$

$$S_{V,CL} = \frac{f_c}{\rho T_{cycle} F_{box}}[SO_2], \tag{7}$$

where: $[OH] = 2 \times 10^6$ molecules cm^{-3}, f_c = conversion factor to convert SO_2 concentration units to $\mu g/m^3$ SO_4, ρ = the dry density of the MBL aerosol (=1.7, see Putaud et al., 2000), k_1 =

10^{-12} cm^3 s^{-1}, T_{cycle} = cloud cycle time = 9 h, F_{box} = fraction of MBL box occupied by the cloud = 0.2.

With [SO_2] ranging between 20 and 200 pptV from clean to polluted conditions (Bates et al., 2000; Mangoni and Putaud, manuscript in preparation), this leads to 8.7×10^{-8} μm^3 cm^{-3} s^{-1}1 $< S_{V,CON} <$ 8.7×10^{-7} μm^3 cm^{-3} s^{-1} and 1.3×10^{-7} μm^3 cm^{-3} s^{-1} $< S_{V,CL} <$ 1.3×10^{-6} μm^3 cm^{-3} s^{-1} and a combined source rate between 2.2×10^{-7} μm^3 cm^{-3} s^{-1} and 2.2×10^{-6} μm^3 cm^{-3} s^{-1}. We can compare this value to the one obtained from the steady state equation for in-situ formed volume, i.e. $S_V = [SO_4]_{CON+CL} \lambda_V$. MSA, which is a tracer for in-situ (biogenic) gas-to-particle conversion, reaches MBL concentrations between 10 and 40 ng/m^3 (Putaud et al., 2000). Taking a MSA yield of 7% in the oxidation of DMS (Putaud et al., 2000), and assuming MSA and SO_4 transfer through identical pathways to the aerosol, this leads to $[SO_4]_{CON+CL}$ = 0.14–0.6 μg/m^3. With λ_V as defined above, we find 5.8×10^{-7} μm^3 cm^{-3} s^{-1} $< S_V <$ 2.3×10^{-6} μm^3 cm^{-3} s^{-1}, well in agreement with our first method. For the base case we take $S_{V,CON+CL} = 10^{-6}$ μm^3 cm^{-3} s^{-1}.

The rate of number transfer to N_{80} is evaluated using typical fitted size distributions for different pollution levels observed at PDH. These size distributions will be discussed in a companion paper (Van Dingenen et al., manuscript in preparation). For each case, we calculated the volume added per time unit from eq. (6), and distributed this over the Aitken and accumulation mode, proportional to the surface area in each mode. This leads to an increase in the $D_{pg,i}$ for each mode which can be calculated from lognormal distribution parameters (see eq. (9) below), keeping N_i and σ_i constant. For grown modes, we then calculate the cumulative number of particles <80 nm, using the lognormal distribution, with $D_{pg,i}$ before and $D_{pg,i}$ after the condensational growth. The difference between the two numbers gives the number of particles that are added to N_{80} due to condensation per unit of time, i.e. the desired rate (eq. (10)). Hence, for both Aitken and accumulation mode:

$$\Delta V_i = k_1 [OH][SO_2] \frac{S_i}{S_1 + S_2} \frac{f_c}{\rho}, \tag{8}$$

$$D_{pgi,new} = \left[\frac{6}{\pi N_i} (V_i + \Delta V_i) \exp\left(-\frac{9}{2} \ln^2 \sigma_{g,i} \right) \right]^{1/3} \tag{10}$$

resulting in a net formation of particles >80 nm:

$$\Delta N_{80} = \sum N_i [F_N(80, D_{pgi}, \sigma_{gi}) - F_N(80, D_{pgi,new}, \sigma_{gi})], \tag{10}$$

with $F_N(D_p, D_{pg}, \sigma_g)$ the cumulative lognormal number distribution fraction at diameter D_p.

With SO_2 varying between 20 and 200 pptV for clean to polluted conditions, this results in a formation rate 5×10^{-5} cm^{-3} s^{-1} $< S_{N,CON} <$ 2.8×10^{-4} cm^{-3} s^{-1} with the highest source rates during polluted conditions. For the base case calculation we adopt $S_{N,CON} = 10^{-4}$ cm^{-3} s^{-1}.

REFERENCES

Ackerman, A. S., Toon, O. B. and Hobbs, P. 1994. Reassessing the dependence of cloud condensation nucleus concentration on formation rate. *Nature* **367**, 445–447.

Bates, T. S., Quinn, P. K., Covert, D. S., Coffman, D. J., Johnson, J. E. and Wiedensohler, A. 2000. Aerosol physical properties and controlling processes in the lower marine boundary layer: a comparison of submicron data from ACE1 and ACE2. *Tellus* **52B**, 258–272.

Bretherton, C. S., Austin, P. and Siems, S. T. 1995. Cloudiness and marine boundary layer dynamics in the ASTEX Lagrangian experiments, II, cloudiness, drizzle, surface fluxes and etrainment. *J. Atmos. Sci.* **52**, 5724–2753.

Fitzgerald, J. W., Marti, J. J., Hoppel, W. A., Frick, G. M. and Gelbard, F. 1998. A one-dimensional sectional model to simulate multicomponent aerosol dynamics in the marine boundary layer (2). Model application. *J. Geophys. Res.* **103**, 16103–16117.

Global Precipitation Climatology Project combined dataset. 1999. http://www.dwd.de/research/gpcc.

Hegg, D. A. and Kaufman, Y. J. 1998. Measurements of the relationship between sub-micron aerosol number and volume concentration. *J. Geophys. Res.* **103**, 5671–5678.

Hinds, W. C. 1982. *Aerosol technology*, Wiley, New York.

Hoell, C., O'Dowd, C., Osborne, S. and Johnson, D. W. 2000. Timescale analysis of marine boundary layer aerosol evolution: Lagrangian case studies under clean and polluted cloudy conditions. *Tellus* **52B**, 423–438.

Hoppel, W. A., Fitzgerald, J. A. and Larson, R. E. 1985. Aerosol size distributions in air masses advecting off

the East Coast of the United States. *J. Geophys. Res.* **90**, 2365–2379.

Hoppel, W. A., Frick, G. M. and Larson, R. E. 1986. Effect of non-precipitating clouds on the aerosol size distribution in the marine boundary layer. *Geophys. Res. Lett*. **13**, 125–128.

Hoppel, W. A., Frick, G. M., Fitzgerald, J. W. and Larson, R. E. 1994. Marine boundary layer measurements of new particle formation and the effects nonprecipitating clouds have on the aerosol size distributions. *J. Geophys. Res.* **99**, 14443–14459.

Hoppel, W. A., Frick, G. M. and Fitzgerald, J. W. 1996. Deducing droplet concentration and supersaturation in marine boundary layer clouds from surface aerosol measurements. *J. Geophys. Res.* **101**, 26553–26565.

Huffman, G. J., Adler, R. F., Arkin, P. A., Chang, A., Ferraro, R., Gruber, A., Janowiak, J., McNab, A., Rudolf, B. and Schneider, U. 1997. The Global Precipitation Climatology Project (GPCP) Combined Precipitation Dataset. *Bull. Americ. Meteor. Soc.* **78**, (1), 5–20.

Murphy, D. M., Anderson, J. R., Quinn, P. K., McInnes, L. M., Brechtel, F. J., Kreidenweis, S. M., Middlebrook, A. M., Posfai, M., Thomson, D. S. and Buseck, P. R. 1998. Influence of sea-salt on aerosol radative properties in the Southern Ocean marine boundary layer. *Nature* **392**, 62–65.

Neusüß, C., Weise, D., Birmili, W., Wex, H., Wiedensohler, A. and Covert, D. 2000. Size segregated chemical, gravimetric and number distribution derived mass closure of the aerosol in Sagres, Portugal during ACE-2. *Tellus* **52B**, 169–184.

O'Dowd, C. D. and Smith, M. 1993. Physicochemical properties of aerosols over the Northeast Atlantic: evidence for wind-speed-related submicron sea-salt aerosol production. *J. Geophys. Res.* **98**, 1137–1149.

Porter, J. N. and Clarke, A. D. 1997. Aerosol size distribution models based on in situ measurements. *J. Geophys. Res.* **102**, 6035–6045.

Pruppacher, H. R. and Klett, J. D. 1978. *Microphysics of clouds and precipitation.* D. Reidel Publishing, Dordrecht.

Putaud, J.-P., Van Dingenen, R., Mangoni, M., Virkkula, A., Raes, F., Maring, H., Prospero, J. M., Swietlicki, E., Berg, O., Hillamo, R. and Mäkelä, T. 2000. Chemical mass closure and assessment of the origin of the submicron aerosol in the marine boundary layer and the free troposphere at Tenerife during ACE-2. *Tellus* **52B**, 141–168.

Raes, F. 1995. Entrainment of free tropospheric aerosols as a regulating mechanism for cloud condensation nuclei in the remote marine boundary layer. *J. Geophys. Res.* **100**, 2893–2903.

Raes, F., Van Dingenen, R., Cuevas, E., Van Velthoven, P. F. J. and Prospero, J. M. 1997. Observations of aerosols in the free troposphere and marine boundary layer of the subtropical north east Atlantic: discussion of processes determining their size distribution, *J. Geophys. Res.* **102**, 21315–21328.

Raes, F., Bates, T. S., McGovern, F. M., Van Liedekerke, M. 2000. The second Aerosol Characterisation Experiment: general overview and main results. *Tellus* **52B**, 111–126.

Seinfeld, J. H. and Pandis, S. N. 1998. *Atmospheric chemistry and physics.* Wiley, New York.

Slinn, W. G. N., Hasse, L., Hicks, B. B., Hogan, A. W., Lai, D., Liss, P. S., Munnich, K. O., Sehmel, G. A. and Vittori, O. 1978. Some aspects of the transfer of atmospheric trace constituents past the air-sea interface. *Atmos. Environ.* **12**, 2055–2087.

Van Dingenen, R., Raes, F. and Jensen, N. 1995. Evidence for anthropogenic impact on number concentration and sulfate content of cloud-processed aerosol particles over the North Atlantic. *J. Geophys. Res.* **100**, 21057–21067.

Van Dingenen, R., Raes, F., Putaud, J.-P., Virkkula, A. and Mangoni, M. 1999. Processes determining the relationship between aerosol number and non-sea-salt sulfate mass concentrations in the clean and perturbed marine boundary layer. *J. Geophys. Res.* **104**, 8027–8038.

Verver, G., Raes, F., Vogelezang, D. and Johnson, D. W. 2000. The second Aerosol Characterisation experiment: meteorological and chemical overview. *Tellus* **52B**, 126–140.